Title

Determination of particle number and brightness using a laser scanning confocal microscope operating in the analog mode

Journal

Microscopy Research and Technique, 71(1)

ISSN

1059-910X

Authors

Dalal, Rooshin B

Digman, Michelle A

Horwitz, Alan F

et al.

Publication Date

2008

DOI

10.1002/jemt.20526

Determination of Particle Number and Brightness Using a Laser Scanning Confocal Microscope Operating in the Analog Mode

ROOSHIN B. DALAL,[1] MICHELLE A. DIGMAN,[2] ALAN F. HORWITZ,[1] VALERIA VETRI,[3] AND ENRICO GRATTON[2]*
[1]*Department of Cell Biology, School of Medicine, University of Virginia, Charlottesville, Virginia 22908*
[2]*Laboratory for Fluorescence Dynamics, Department of Biomedical Engineering, University of California, Irvine, California 92697*
[3]*Dipartimento di Scienze Fisiche ed Astronomiche, Università di Palermo, Italy*

KEY WORDS image correlation spectroscopy; FCS; molecular aggregation; live cell imaging

ABSTRACT We describe a method to obtain the brightness and number of molecules at each pixel of an image stack obtained with a laser scanning microscope. The method is based on intensity fluctuations due to the diffusion of molecules in a pixel. For a detector operating in the analog mode, the variance must be proportional to the intensity. Once this constant has been calibrated, we use the ratio between the variance and the intensity to derive the particle brightness. Then, from the ratio of the intensity to the brightness we obtain the average number of particles in the pixel. We show that the method works with molecules in solution and that the results are comparable to those obtained with fluctuation correlation spectroscopy. We compare the results obtained with the detector operating in the analog and photon counting mode. Although the dynamic range of the detector operating in the photon counting mode is superior, the performance of the analog detector is acceptable under common experimental conditions. Since most commercial laser scanning microscopes operate in the analog mode, the calculation of brightness and number of particles can be applied to data obtained with these instruments, provided that the variance is proportional to the intensity. We demonstrate that the recovered brightness of mEGFP, independent of concentration, is similar whether measured in solution or in two different cell types. Furthermore, we distinguish between mobile and immobile components, and introduce a method to correct for slow variations in intensity. *Microsc. Res. Tech. 71:69–81, 2008.*

INTRODUCTION

Determining the state of aggregation or clustering of molecules in living cells is a matter of increasing importance and interest. For example, in response to external stimuli, many membrane receptors are thought to initiate signaling events by aggregation (Miyamoto et al., 1995; Schlessinger, 2000). However, despite the importance and ubiquity of this notion, it has not been shown directly for most receptors and contrary evidence has been presented for others (Kim et al., 2004; Moriki et al., 2001; Shi and Boettiger, 2003). Furthermore, the degree of clustering in most cases has not been quantified. Methods based on fluctuation spectroscopy provide a powerful approach for detection and quantification of protein aggregation (Chen et al., 2002). Moment analysis, the photon counting histogram, and correlation methods are all capable of determining the number and degree of aggregation of cellular molecules. One goal is to extend these technologies to confocal images from analog systems, since they provide highly resolved spatial and temporal changes and are used in many biology laboratories.

We have approached this issue using moment analysis, also referred to as Number and Brightness (N&B) analysis, for each pixel in an image stack. From the average intensity in each pixel and the variance of the intensity distribution, the number and brightness (aggregation) of mobile particles is determined, thereby providing a new contrast mechanism in the images based on a molecular property. However, this analysis is complicated by the detectors used on confocal microscopes, since in the N&B analysis the variance of the intensity distribution due to the detector statistics must be equal to the average intensity. This assumption appears to be satisfied for a photon counting detector (Digman et al., in press) (It is common practice to assume that for a photon counting detector the shot noise is given by the square root of the number of counts.). However, in this study, we show that the variance of a detector operating in the analog mode is linearly proportional to the average intensity plus a small intercept value. Using such a model we developed a system of equations specific for analog detectors to obtain the particle brightness and the number of particles at each pixel. We verified this analysis with measurements using molecules

*Correspondence to: Enrico Gratton, Laboratory for Fluorescence Dynamics, Department of Biomedical Engineering, University of California, Irvine, CA 92697, USA. E-mail: egratton22@yahoo.com

Received 27 July 2007; accepted in revised form 8 August 2007

Contract grant sponsor: Cell Migration Consortium; Contract grant number: U54 GM64346; Contract grant sponsor: NIH; Contract grant number: P41-RRO3155.

DOI 10.1002/jemt.20526

Published online 15 October 2007 in Wiley InterScience (www.interscience.wiley.com).

in solution, where we determined the number of molecules and the brightness at each pixel based on the distribution of digital level (DL) obtained for a stack of images. These solution experiments show that, when properly characterized, an analog detector, which is common in most of the commercial laser confocal microscopes, can be used to provide accurate determinations of the number and brightness of molecules in solution and in cells. A limitation of analog detection is that the dynamic range is smaller that that of a detector operating in the photon counting mode because of the analog-to-digital converter resolution. Ultimately, the dynamic range allows quantitative determination of the size of aggregates that are within a factor of 2–10 in brightness.

MATHEMATICAL BACKGROUND

The N&B Analysis Using an Analog Detector

Given a stack of 10–100 images, we extract the intensity values as a function of the frame number for every pixel of the image. We define the average intensity $\langle k \rangle$ and variance σ^2 according to the following formulas:

$$\langle k \rangle = \frac{\sum_i k_i}{K} \tag{1}$$

$$\sigma^2 = \frac{\sum_i (k_i - \langle k \rangle)^2}{K} \tag{2}$$

where k_i is the intensity at a given pixel and K is the number of frames analyzed. The ratio of the variance to the average intensity (in one pixel) is different if few bright particles diffuse across the laser illumination volume compared to the situation in which many dim particles are diffusing. We assume that the variance of the intensity distribution is due to the combination of two terms, that is, the variance due to the occupation number (σ_n^2) and the variance due to the count statistics or shot noise (σ_d^2) of the detector.

We have shown that the variance due to the occupation number is proportional to the square of the molecular brightness (Digman et al., in press). The average brightness ε of a given molecule is defined as the number of photons measured per second per molecule when the molecule is at the center of the profile of illumination. This definition follows the common definition of brightness in the fluctuation spectroscopy literature (Chen et al., 1999). Of course, the molecular brightness depends on the laser power at a given wavelength, the detection efficiency and the molecule quantum yield. The average number of molecules, n, refers to the average number of molecules in the illumination profile. To convert the average number of molecules to concentrations, we need to calibrate the volume of illumination.

The current generated by the photomultiplier is proportional to the photons that are detected by the cathode once the dark current has been subtracted. The proportionality constant S is the average conversion factor between one photon detected and the number of DLs produced by the electronics. The knowledge of S will allow us to directly express the molecular brightness in terms of photons/s/molecule in the analog system. This approach allows us to compare different instruments and detectors.

We used two methods to measure S for a particular detector and detector settings such as gain and offset. One is to measure the variance due to the detector in the absence of number fluctuations for different amounts of current. This can be done by allowing the detector to see a source of steady illumination. Under this condition, a plot of the variance as a function of the average signal is linear, has a slope equal to S, and an intercept equal to a term which is related to the readout noise of the analog system. This method is very useful because it also gives the range of intensities over which the system behaves linearly. The other is to measure the distribution of DL due to single photons using a regime in which only a few photons are detected. For example, one can measure the histogram of DL of the dark current for the photomultiplier detector. This method provides the parameter S and the readout noise parameter, as well as the offset of the analog electronics which is needed to properly calculate the true intensities.

When we measure the current of the analog detector with a certain integration time given by the analog electronics, the variance and the signal are given by the following expressions:

$$\sigma_n^2 = S^2 \varepsilon^2 n \tag{3}$$

$$\sigma_d^2 = S^2 \varepsilon n + \sigma_0^2 \tag{4}$$

$$\langle k \rangle = S \varepsilon n + \text{offset} \tag{5}$$

where ε is the molecular brightness in photon/s/molecule, n is the number of molecules in the excitation volume, and the offset is a constant quantity characteristic of the specific detector setting. The aforementioned equations assume that the only source of fluctuations is due to the particles crossing the excitation volume [Eq. (3)], and the variance of the detector current in the absence of number fluctuations [Eq. (4)] is linearly proportional to the current plus the readout noise term σ_0^2. Similar equations, excluding the S factor that converts photon counts into DL, were used for photon counting detectors (Digman et al., in press).

Once the readout noise term σ_0^2 is independently determined, we can subtract its value from the measured variance at one pixel, so that the residual variance only contains terms related to particle fluctuations and the intrinsic detector noise. In the majority of analog systems, the photomultiplier current is added with an offset. This offset has no variance since it is constant for a given setting of the detector amplifier. The offset must be subtracted from the measured intensity to obtain the true sample intensity. We define the parameter B (apparent brightness) for each pixel as the ratio of the variance to the average intensity and N (apparent number of particles) as the ratio of the total intensity to B.

$$B = \frac{\sigma^2 - \sigma_0^2}{\langle k \rangle - \text{offset}} = \frac{S^2\varepsilon^2 n + S^2\varepsilon n}{S\varepsilon n} = S(\varepsilon + 1) \quad (6)$$

$$N = \frac{(\langle k \rangle - \text{offset})^2}{\sigma^2 - \sigma_0^2} = \frac{\varepsilon n}{\varepsilon + 1} \quad (7)$$

Note that B depends only on the particle brightness and is independent of the number of particles. The expressions for n and ε for the analog detector can be obtained in terms of the intensity and variance at each pixel from Eqs. (6) and (7) and they are shown as follows:

$$n = \frac{(\langle k \rangle - \text{offset})^2}{\sigma^2 - \sigma_0^2 - S(\langle k \rangle - \text{offset})} \quad (8)$$

$$\varepsilon = \frac{\sigma^2 - \sigma_0^2 - S(\langle k \rangle - \text{offset})}{\langle k \rangle - \text{offset}} \quad (9)$$

Determination of the Analog Detector Characteristics

From the point of view of the N&B analysis, we characterize the detector by three quantities, the offset, the factor S between photon counts and DL, and the readout variance, σ_0^2. To determine these three parameters, we need to perform two separate measurements. In one measurement we determine the intercept and the slope from the variance versus intensity plot when the detector is illuminated with various amounts of steady light. We still need to measure the detector offset, which is obtained from a measurement of the dark current.

Figure 1A shows the distribution of dark counts for one of the detectors of the Olympus FV1000. With respect to the N&B analysis, the particular shape of the one-photon distribution (Fig. 1A) is irrelevant. The requirement that the variance due to the detector be proportional to the intensity will always be satisfied if the detection of individual photons is independent of the number of photons detected. The ratio between the variance and the intensity due to the detector is always constant unless there is saturation of the detector (amplifier or analog-to-digital converter), and the offset remains constant and independent of the intensity. Figure 1B shows the plot of the variance as a function of intensity for a sample in which number fluctuations are absent (a blank coverslip illuminated with different laser powers). The analog detector behaves linearly over the range of our measurements. However, this range is limited by the specific analog-to-digital converter (12 bit A/D converter, 4,096 levels in our instrument). Because the offset that is about 130 DL and the broad distribution of DL (Fig. 1A), we start to see saturation when the average signal is about 2,000 DL or higher. This limited dynamic range determines the maximum brightness ratio that we will be able to measure. This is in contrast to the detector operating in the photon counting mode that has a much wider dynamic range (>1,000) as shown in Digman et al. (in press). The slope and intercept of the variance versus intensity plot, shown in Figure 1B, allows us to calculate the parameters for this detector: S = 52.0 DL/photon, σ_0 = 7.51 DL and offset = 130.7 DL. Note that the detector offset is the value corresponding to the histogram minimum. Frequently, DL much lower than the offset is obtained. These values are due to a characteristic undershoot of the single photon response due to underdamping of the analog circuit. Therefore, the offset does not correspond to the minimum DL, but to the DL in the absence of detected photons.

Effect of the Detector Stability on the Determination of ε and n

The stability of the parameter S, as well as the offset, is critical for determining the molecular brightness and number of particles. The value of the readout variance is also important at low light levels. Since in Eq. (6) the ratio B/S is very close to 1, a small change in S or the detector readout variance results in a relatively large effect on the particle number and brightness. Furthermore, for the determination of n and ε, the detector offset has a large influence. If the offset is not constant during the acquisition of the stack or among different measurements, the recovered values of ε and n will be strongly affected. We found that the value of S is relatively constant from day-to-day but that the offset shows variations of several DL over a period of hours (Figs. 1C–1E). These variations are caused by temperature fluctuations, the amount of time the detector has been operating that day, etc. For example in Figures 1C–1E, the temperature of the room changed at t = 76 min when another laser in the room was turned off. The effect on the offset is apparent while the effect on the S factor is minor. As an example of the effect of changes in offset and S on the determination of ε and n, we use a data set from the evaluation of mEGFP brightness in solution. At a nominal laser power of 1%, for the conditions of that particular experiment, the offset was 134 DL and S = 304 DL/photon. The recovered values for the solution experiments were n = 3.48 molecules and the brightness was 9,770 counts/s/molecule. If the value of the offset differed by 1% of the value assumed, the relative changes in n and ε changed by −18% and +17%, respectively. If the S factor changes by 1%, the changes in n and ε are +16% and −18%, respectively. From the data of Figures 1C–1E, we can see that changes of the order of 1% in offset, S, and readout noise are to be expected for our detectors over the course of about 1 h. Consequently, accurate recovery of n and ε requires that a dark current measurement be made directly before and/or after acquisition of a data to obtain sufficiently accurate values of the detector offset. Even with continuous calibration and monitoring of the offset and S value, we estimate that the absolute values of the n and ε recovered from a single measurement can vary by up to 20%. This error is adequate to distinguish between the brightness of a monomer from that of a dimer. Of course, these considerations only apply to the absolute values, while the determination of the relative values across an image can be done with greater precision.

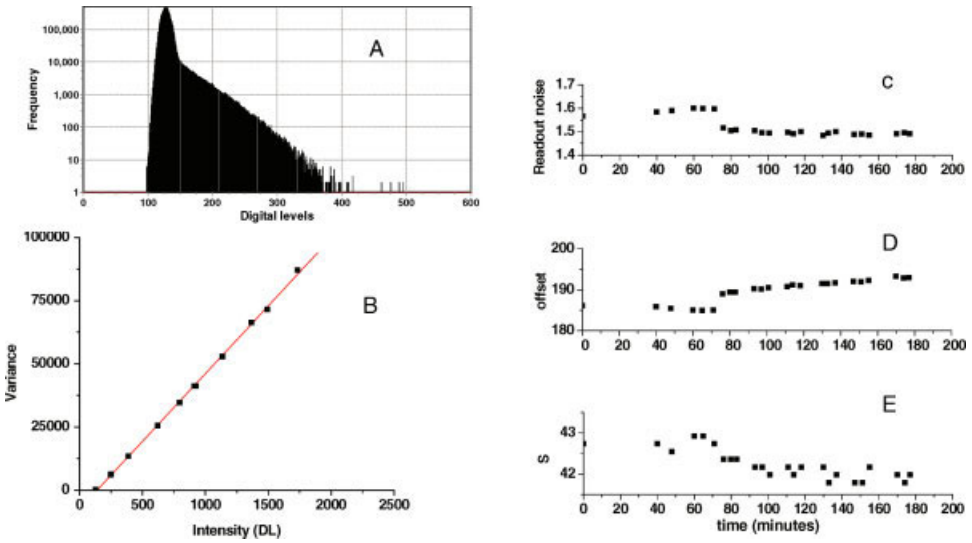

Fig. 1. (**A**) Dark current distribution of DL of one of the photomultipliers of the Olympus FV1000. The Gaussian peak at about 130 DL is used to calculate the offset (the center of this Gaussian part) and the readout noise (the standard deviation of the distribution when no photons are detected). The slope of the exponential part of the distribution is used to calculate the parameter S, the conversion factor between DL and photons. (**B**) Measurement of the ratio of the variance versus intensity for a sample that has no particle number fluctuations. The response of the detector is linear. The slope of this plot is also used to determine S. (**C–E**) Measurements of the stability of readout noise, offset, and S as a function of time for one detector of the Olympus FV300 microscope. [Color figure can be viewed in the online issue, which is available at www.interscience.wiley.com.]

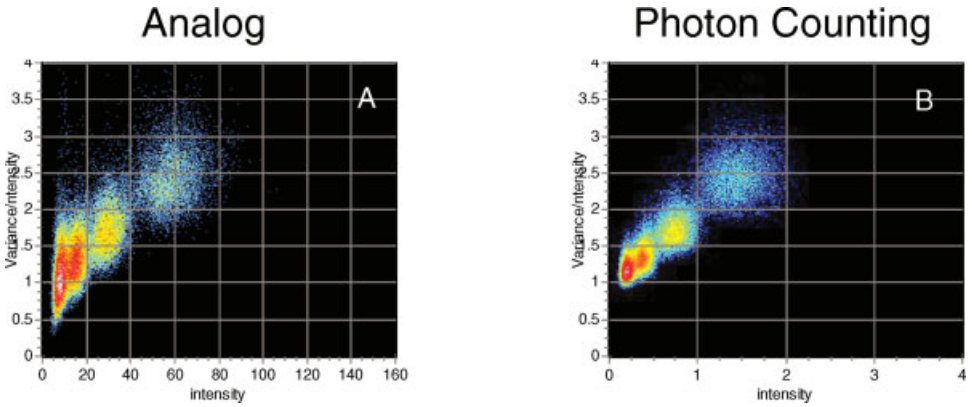

Fig. 2. (**A**) Simulation of pixel distribution of the parameter B/S as a function of the intensity for the analog detector. (**B**) Simulation of pixel distribution of the parameter B for the photon counting detector. At low intensity, the vertical spread of the histogram for the photon counting detector is narrower than for the analog detector. [Color figure can be viewed in the online issue, which is available at www.interscience.wiley.com.]

Effect of the DL Distribution of the Analog Detector on the (Pixel) Precision Determination of the Particle Number and Brightness

The DL distribution added by the analog detector electronics is a large part of the signal fluctuation. This distribution is absent in the detector operating in the photon counting mode, since for this mode of operation one photon always gives one count. Therefore, achieving a given (pixel) precision in the determination of ε and n using the analog mode of detection requires sufficient statistics. We performed a simulation of the analog detector and of the photon counting detector to analyze the effect of the DL distribution on the precision of the determination of ε and n. In the simulation of Figure 2, we show the 2D histogram of the B/S ($S = 1$ for the photon counting detector) parameter as a function of the average pixel intensity for four values of particle brightness differing from each other by a factor of 2. This simulation used 100 frames. The "sharpness" of the distribution along the vertical axis gives an idea of the pixel standard deviation in the determination of the brightness. The analog detector adds a relatively wide distribution to the original intensity distribution (which is due to the intrinsic Poisson statistics of the detector, both in the analog or in the photon counting mode). For the photon counting detector, samples that differ in brightness by a factor of 2 are well separated in the vertical scale (proportional to the brightness),

while for the analog detector the two distributions overlap. Thus, it appears possible to recover small differences in brightness when using analog detectors by integrating for a longer time than when using photon counting detectors or by averaging neighboring pixels to increase the local statistics. Note that this discussion only refers to pixel statistics, while the average brightness can be recovered with relatively good precision in both cases.

Separation of the Mobile and the Immobile Fraction

According to Eq. (6), the parameter B in the absence of fluctuating particles is equal to S. If we represent the value of B/S for every pixel of an image, we should be able to recognize the pixels with immobile features ($B/S = 1$) from the pixels with mobile components ($B/S > 1$). Generally we display the 2D histogram of the values of B/S versus intensity. In this histogram, all points with immobile fractions are easily recognized and then identified in the image. In pixels with both mobile and immobile components, the apparent brightness is always less than the brightness of the mobile component because of the combination of the $B/S > 1$ value of the particle with the $B/S = 1$ value of the immobile component. If R is the ratio between the immobile to the mobile fractional intensity at one pixel, then the expression for the brightness with both mobile and immobile part is

$$\varepsilon_m = \frac{\varepsilon}{1+R} \tag{10}$$

where ε_m is the measured brightness and ε is the brightness in the absence of the immobile part. For pixels with an immobile fraction it is generally true that the intensity due to the immobile part is much larger than the intensity due to the mobile part. Therefore in pixels with an immobile fraction, B/S tends to 1 since ε tends to zero. The apparent number of particles in pixels with an immobile fraction increases due to the added intensity of the immobile part and to the lower apparent brightness in these pixels.

$$n_m = n(1+R) + \frac{I_{im}(1+R)}{\varepsilon} \tag{11}$$

where n_m is the measured apparent number of particles, R is the ratio of the immobile to the mobile intensity, and I_{im} is the intensity (in counts/s) of the immobile part.

MATERIALS AND METHODS

Molecular Biology

We generated a nondimerizing point mutant of EGFP (A206K) (Zacharias et al., 2002), termed monomeric EGFP (mEGFP), from the pEGFP-N1 vector (Clontech) using the Quickchange site-directed mutagenesis kit (Stratagene, La Jolla, CA) according to the manufacturer's instructions, using primers as previously described (Zacharias et al., 2002). For solution experiments, we introduced the mutation into the pET-21-day(+) bacterial expression vector encoding EGFP, and purified the mEGFP as previously described (Digman et al., in press).

Sample Preparation

Yellow-green fluorescent 100-nm beads (Fluospheres, carboxylate modified) (Molecular Probes, Eugene, OR) were immobilized onto a glass-bottomed dish by dissolving the beads in ethanol and allowing a drop of the bead solution to air dry at room temperature. Fluorescein was purchased from Sigma (St Louis, MO) and stored as a stock in dilute NaOH. The concentration of a working stock solution was calculated using the absorbance at 494 nm and an extinction coefficient of 75,000 cm^{-1} M^{-1}. Dilutions from this measured stock were subsequently prepared in 100 mM Tris buffer (pH 9.0) and protected from room light. The concentration of a stock solution of mEGFP was calculated using the absorbance at 486 nm and an extinction coefficient of 58,000 cm^{-1} M^{-1}. Dilutions from this stock were subsequently prepared in 100 mM Tris buffer (pH 9.0) containing 1% defatted Bovine Serum Albumin (BSA). To prevent adsorption to the coverslip, measurements of mEGFP in solution were performed in Lab-Tek chambered coverglass (Campbell, CA) precoated with sterile 1% defatted BSA for 1 h at 37°C. Background counts were acquired using the 1% BSA buffer alone.

Cell Culture

The CHO K1 cell line was maintained in low glucose Dulbecco's minimum essential medium (DMEM) supplemented with penicillin/streptomycin, 10% Fetal Bovine Serum (FBS), and nonessential amino acids. Murine embryonic fibroblasts (MEF) were maintained in high glucose DMEM supplemented with 10% FBS. Cells were maintained in an incubator at 37°C with an 8.5% CO_2 atmosphere. Cells were lifted with 0.05% Trypsin-EDTA and plated in CCM1 medium (Hyclone, Logan, UT) buffered with 15 mM HEPES on homemade 35-mm glass bottomed dishes as previously described (Laukaitis et al., 2001). The dishes were precoated with either 1 or 2 μg/mL fibronectin (Sigma) and maintained at 37°C during imaging with a Warner Instruments heated stage insert (Warner Instruments, Hamden, CT) and a Bioptechs (Bioptechs, Butler, PA) objective heater. CHO K1 cells were transiently transfected with pmEGFP-N1 using Lipofectamine (Invitrogen, Carlsbad, CA) 24 h prior to imaging. CHO K1 cells and MEF cells stably expressing mEGFP were generated by transient transfection with lipofectamine, positive selection for 2 weeks in the presence of 1 mg/mL neomycin sulfate (G418), and a sort for low and medium expressing cells using a fluorescence-activated cell sorter.

Microscopy and Image Analysis

Confocal images were either collected on an Olympus Fluoview 300 LSCM built around an IX70 inverted microscope or on an Olympus Fluoview 1000 LSCM built around an IX81 inverted microscope. Both were fitted with a 60× PlanApo (1.40 NA) oil immersion objective. The analog detector (PMT) was used in the range of 700–800 V with 1× gain and 0% offset. Images of solutions and cells were collected with resolutions of either 46 or 92 nm/pixel. A region of interest, e.g., clip box of 256 × 256 pixels was generally acquired from an image of 512 × 512 pixels. The pixel dwell time was

8 μs/pixel and the pinhole diameter was 200 um (setting 4 out of 5 on the Olympus FV300). Excitation was from the 488-nm line of a 40 mW argon ion laser.

Correction for Bleaching

If the intensity at one location slowly changes due to bleaching, the variance at that location has an extra term in addition to the number fluctuation variance. We assume that only the immobile part is bleached. This drift of the average intensity can be corrected using different techniques. As previously described (Digman et al., in press) we use a high-pass filter to the intensity as a function of time of each pixel to remove slowly varying signals. After removal of the trend, we add a constant equal to the average intensity at that pixel. Therefore, the variance of the "immobile" part is unaffected by bleaching after correction and we can recover the variance of the mobile part.

Data Analysis

Data presentation and analysis was done using the N&B analysis screen of the SimFCS program (www.lfd.uci.edu). Briefly, the analysis implements Eqs. (6) and (7), or (8) and (9). Generally, Eqs. (8) and (9) are used for solution samples. For the analog system, the operator must enter the values of S, the offset, and the readout noise. The offset and the readout noise are determined by the histograms of dark count. For the value of S, we can perform a calibration using a sample without particle fluctuations or directly from the dark count histogram if the DL histogram is relatively well described by an exponential. All these operations are automatic and all calculations occur during the time of data display. There are various maps available, the intensity map, the brightness map, the number of particle map, and the 2D histograms. A cursor can be moved in the histogram window to allow for examination of specific areas in the image and specific parameter values can then be recorded or exported for further processing. Simulations were also performed using the SimFCS program as described in Digman et al. (in press).

RESULTS

Solution Measurements

To test the ability of our system to accurately recover the number of particles and their brightness, we performed a dilution experiment with a solution of mEGFP. A stock solution of mEGFP was diluted in steps from 400 nM down to 4 nM. For each dilution, an image stack of 50 frames was acquired, and additional 50 frames with no excitation light (dark current) were acquired immediately after each image stack and correction factors were obtained from the dark current. Equations (8) and (9) were used to recover n and ε from each image stack. Note that the detector offset must be subtracted before the calculation of n and ε. The recovered B/S values for mEGFP remain stable and independent of the protein concentration (Figs. 3A and 3B). In panel A of Figure 3 we also verified that for a fixed sample, the value of B/S remains constant at around 1 as the laser intensity is increased. In Figure 3C we report the measurement of the brightness ε in units of counts/s/molecule (cpsm). When the concentration was 10 nM or lower, the brightness was slightly underestimated. The average brightness was 28,400 cpsm with a standard deviation of 1,000 cpsm with the lowest concentration excluded. Figure 3B demonstrates that the recovered number of particles decrease linearly with decreasing concentration. At the lowest concentration of 4 nM, the number count was slightly overestimated. Concentrations below this range were difficult to measure, because the variance due to the detector statistics dominates the total variance, while concentrations above this range begin to saturate the detector.

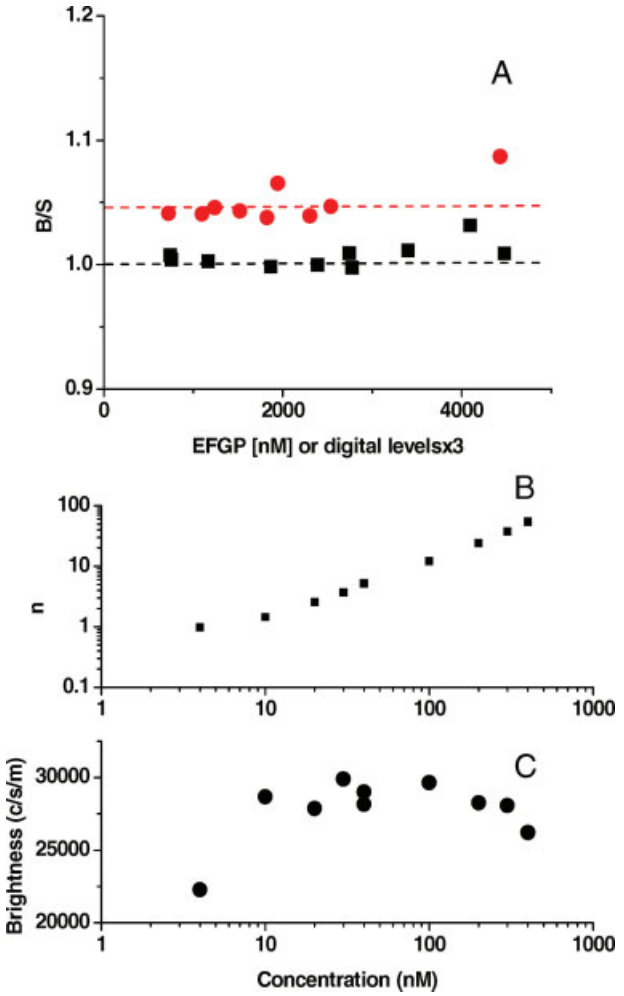

Fig. 3. (**A**) Measurement of the parameter B/S for a solution of mEGFP at different concentrations (●) and for a fixed slide sample (■) as a function of the laser illumination. (**B**) As the concentration of mEGFP increases the number of molecules increases. Below 10 nM, the recovery of the number of molecules is affected by a larger error. (**C**) As the concentration of the solution increases, the recovered brightness remains constant. Below 10 nM, the recovery of the brightness values is affected by a large error. [Color figure can be viewed in the online issue, which is available at www.interscience.wiley.com.]

We also measured the effect of laser power intensity on the recovery of brightness and number count. Using a sample of mEGFP diluted to ~100 nM, we acquired image stacks at various laser powers. In Figure 4B the brightness of the mEGFP solution increases linearly with increasing laser power, as expected. On the x axis we plot the intensity in counts/s rather than the laser

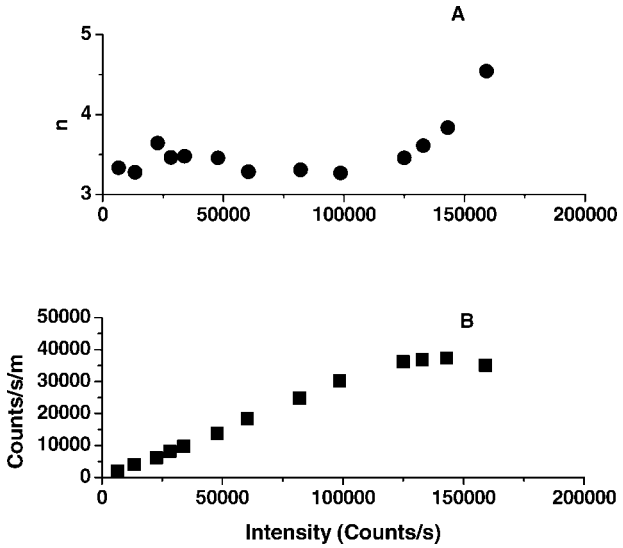

Fig. 4. Hundred nanomolar mEGFP in solution. (**A**) The recovered number of molecules remains constant until a saturation is reached at 120,000 counts/s corresponding to about 5% of the laser power. (**B**) The recovered brightness increases linearly with laser power until saturation is reached.

power, to emphasize that the saturation we observe is a physical phenomena in which the variance is no longer proportional to the intensity rather than being due to a nonlinearity of the Acousto-Optic Tunable Filter (AOTF) used to select the laser power in the Olympus system. The counts were saturated when more than 5% laser power was used; this corresponds to $\sim$120,000 c/s. In Figure 4A we also demonstrate that the number count remains constant over the powers used until saturation is reached.

These experiments show that an analog instrument can be used to accurately recover the brightness with a protein like mEGFP and suggest that a commercial laser scanning microscope could be used to measure the aggregation of proteins in cells.

Effect of the Number of Frames Acquired on the Precision of the Measurement of n and ε

To determine the number of frames required to reach a given precision, we acquired 300 frames of a solution of mEGFP and then analyzed the stack by dividing the entire record in pieces of 20, 40, 80, and 160 frames each (Fig. 5). The pixel 2D values of B/S versus intensity are shown in Figures 5A–5E. For each of the images, the B/S histogram was fit using a Gaussian,

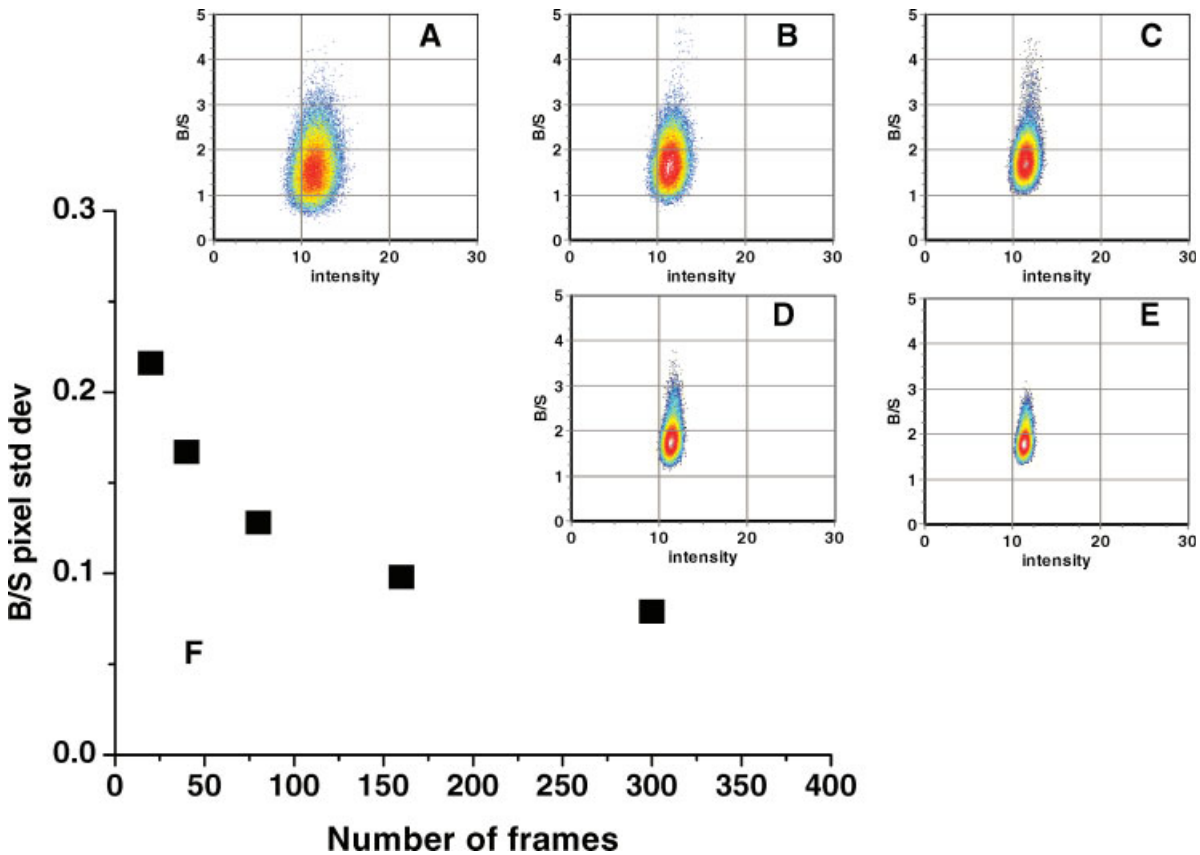

Fig. 5. Recovery of the brightness and number of particles using different number of frames. A solution of 100 nM EGFP was measured using 300 frames, 8-ms pixel dwell time. The sequence was then analyzed dividing the set in pieces of 20, 40, 80, 160, and 300 frames as shown in panels **A–E**. The error plotted in (**F**) is the standard deviation of the measurements in A–E. [Color figure can be viewed in the online issue, which is available at www.interscience.wiley.com.]

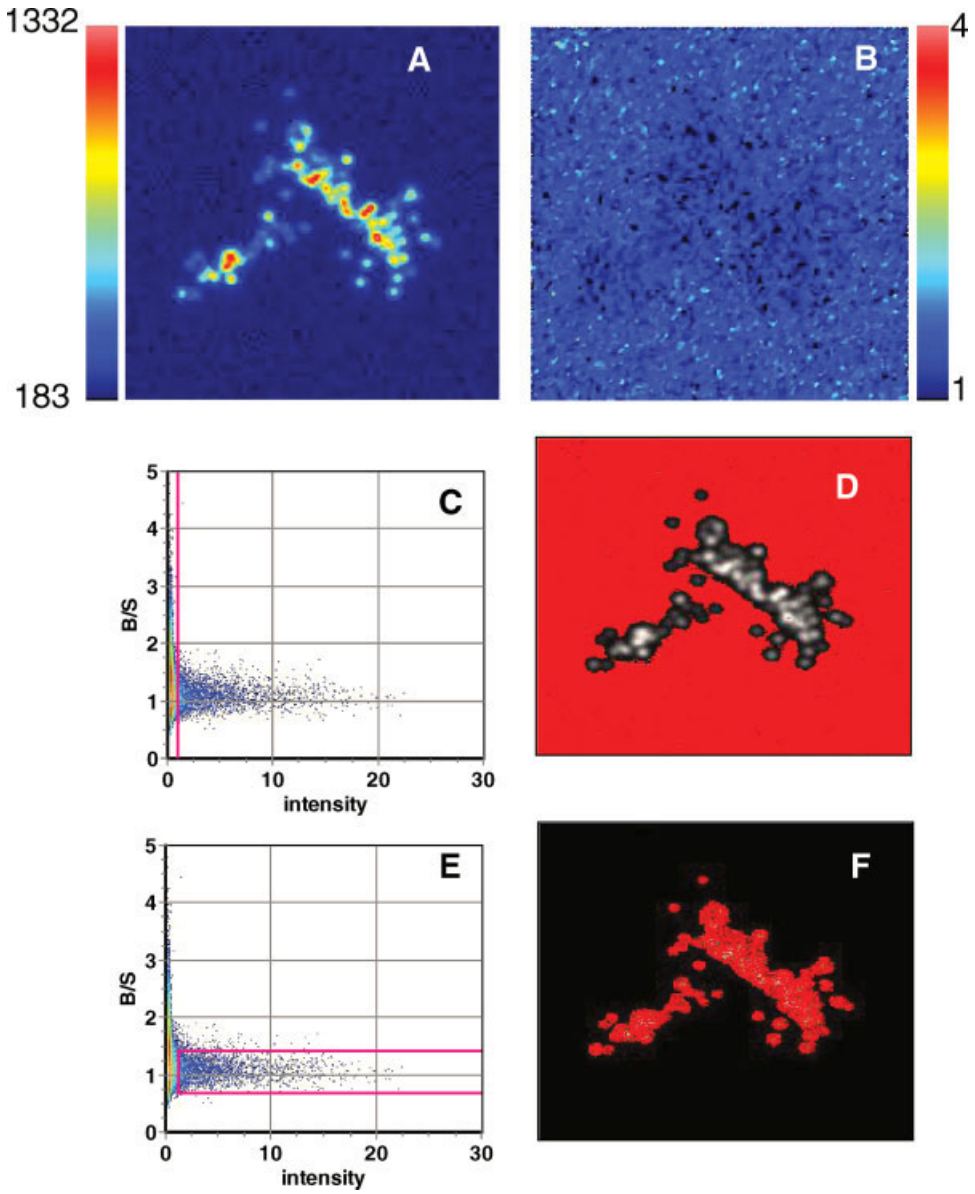

Fig. 6. Fluorescent beads immersed in a 100 nM fluorescein solution. (**A**) Map of the average intensity of the immobilized beads. (**B**) The *B*/*S* value of the beads is around 1, while the *B*/*S* value of the fluorescein part is larger than 1. By selecting the low intensity part of the 2D histogram as shown in (**C**), the points within the rectangle map to the fluorescein solution as shown in (**D**). If we select the part of the histograms corresponding to a ratio *B*/*S* around 1 (**E**), we select the beads (**F**). The image size is 11.8 μm^2.

and the standard deviation is shown in Figure 5F. As the number of frames in the set increases, the error in the *B*/*S* value decreases by the square root of the number of frames utilized. Although the center of the distribution is accurately determined even with 20 frames, the standard deviation is quite large. Therefore, if there are regions of different brightness in the cell it will be difficult to reach a "pixel" resolution of the brightness. However, since there is oversampling in all our images (about nine pixels map to the same point spread function in the radial direction), the average of the *B*/*S* value in these pixels will reduce the error by the square root of the pixels that are averaged, thus substantially reducing the brightness indetermination and allowing separation of neighboring regions with different brightness.

Identification of the Immobile Fraction

One of the advantages of our analysis is the ability to distinguish mobile from immobile components. We demonstrated this by creating a sample in which both mobile and immobile components are present but are spatially separated (fixed fluorescent beads immersed in a fluorescein solution). An image stack of 50 frames was acquired followed by additional 50 frames of dark current. Figure 6A shows the intensity image of a few bead aggregates, with the lower intensity fluorescein surrounding them. The map of *B*/*S* is shown in Figure 6B. Although the differences between the fluorescein (with *B*/*S* larger than 1, Fig. 6C) and the beads (with *B*/*S* around 1, Fig. 6E) are not easily seen in *B*/*S* image, examination of the 2D histograms of variance/

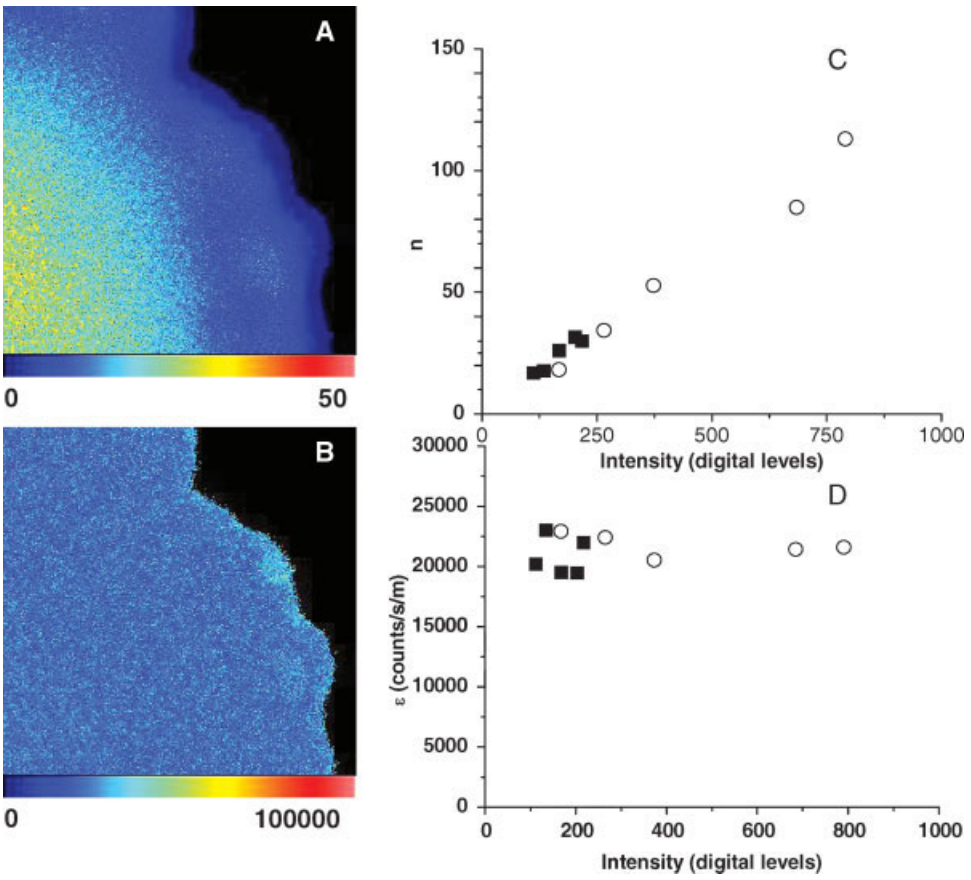

Fig. 7. Measurement of n and ε in CHO-K1 (open symbols) and MEF (closed symbols) cells expressing mEGFP. For any given image, the brightness map is relatively constant (**B**) while the number of molecules varies according to the cell thickness (**A**). In panel **C** and **D** the recovered values of n and ε are plotted as a function of the average fluorescence intensity of the image for a series of cells. The recovered brightness is relatively constant while the number of particles scales with the average fluorescence intensity in each cell. The image size is 29.4 μm^2.

intensity versus intensity clearly reveals the separation of immobile components from mobile ones. The pixels selected by the pink rectangles identify the location of the mobile fluorescein molecules, highlighted in Figure 6D, and the immobile beads, highlighted in Figure 6F.

Measurements in Cells

mEGFP in Cells. We made measurements of brightness and particle count in living cells. CHO K1 and MEF cells expressing mEGFP were imaged, and stacks of 50 frames were acquired along with 50 frames of dark current. Figures 7A and B show an example in which the center of a cell is located in the bottom left hand corner. A map of the number count is shown in Figure 7A and reveals a monotonic decrease in N value outward from the thick nuclear and perinuclear regions toward the thinner lamellipodia region. On the other hand, since mEGFP remains in a monomeric form throughout the cytosol of the cells, we recover a uniform brightness throughout the cell as shown on the B map in Figure 7B. By making measurements on several different cells stably expressing mEGFP, we were able to recover brightness and number counts over a range of protein concentrations (intensities). Although the MEF cells expressed less protein than the CHO cells, the number count as shown in Figure 7C remains linearly proportional to concentration in both cell types. Figure 7D demonstrates that the brightness of mEGFP is stable and independent of expression level over a range of concentrations. The average ε value of mEGFP in the cells was 21,300 cpsm with a standard deviation of 1,300 cpsm. This value is similar to the value of 28,400 cpsm obtained from mEGFP in solution using the same laser power. We believe that the difference between the brightness value in solution and the brightness in the cell could be due to some immobile fraction present in the cell. According to Eq. (10) a 1:3 ratio of the immobile to mobile fraction could explain the observed difference.

Effect of Bleaching Correction on Brightness and Number Count

Photobleaching of fluorophores is a common problem in live cell imaging, and can dramatically alter the recovered brightness and number count values. As mentioned previously, bleaching adds an additional variance term to the total variance. This will result in an overestimation of the true brightness, and an underestimation of the true number count, as predicted by Eqs. (8) and (9). Similarly, cell movement or protrusion/retraction events will slowly change the intensity at the affected pixel. All these processes will contribute to the pixel variance as discussed in the mathematical background. To demonstrate the effect of detrending correction in cells, we intentionally introduce a photobleaching artifact by imaging a CHO K1 mEGFP-expressing cell with high laser power. Without correction, the recovered brightness is 41,200 cpsm, larger than expected due to the extra variance contri-

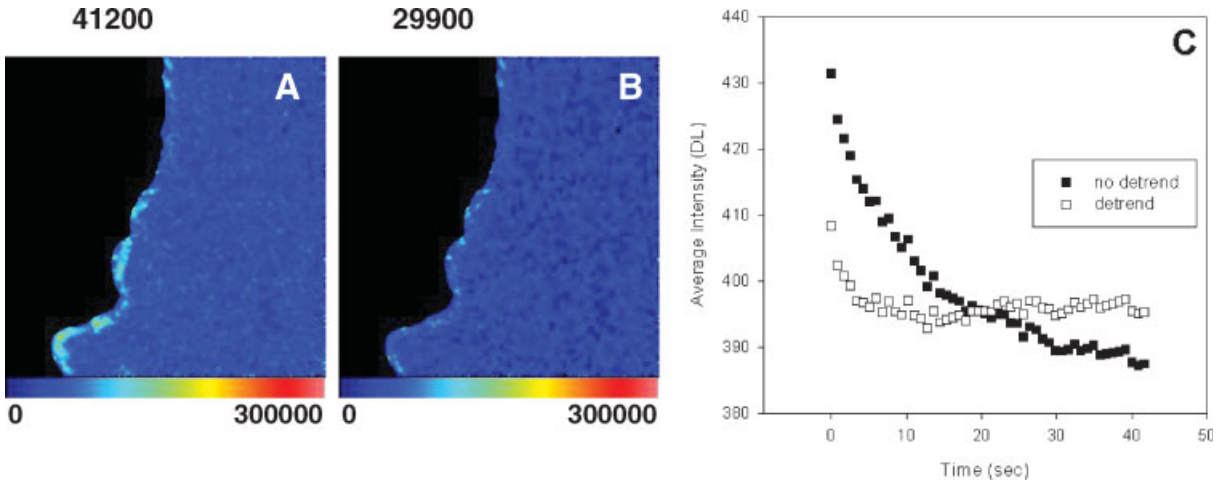

Fig. 8. Example of photobleaching correction in a CHO K1 cell expressing mEGFP. (**A**) The brightness map before correction. The average recovered brightness is 41,200 cpsm. (**B**) The brightness map after bleaching correction. The average recovered brightness is now 29,900 cpsm. (**C**) The average frame intensity decreases considerably when bleached (filled squares), but the correction algorithm restores the average value of the intensity. The image size is 23.5 μm^2.

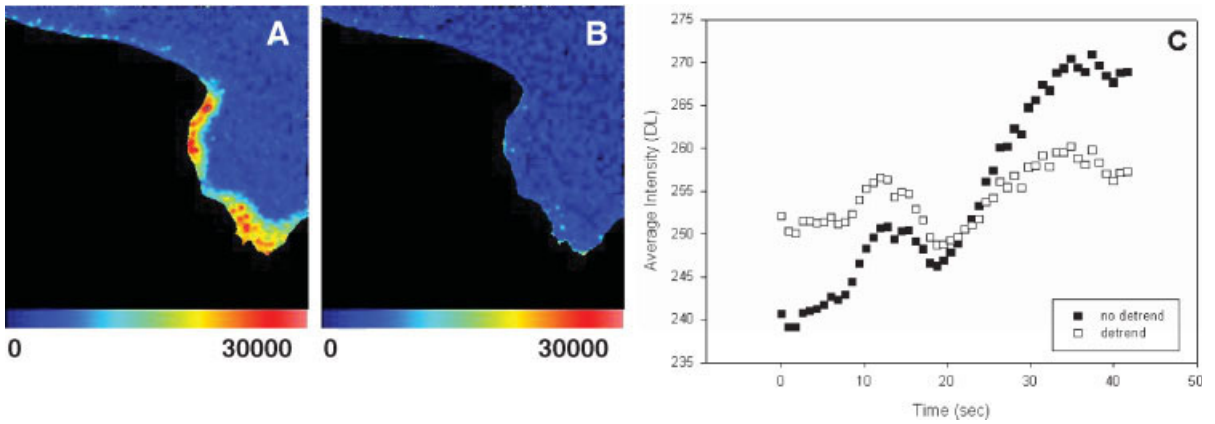

Fig. 9. Example of cell protrusion artifact correction for a CHO K1 cell expressing mEGFP. (**A**) The brightness map before correction reveals two areas of abnormally high brightness where small protrusions occurred. (**B**) After detrending, all regions of the cell have a uniform brightness, even in areas where membrane motion took place. (**C**) A plot of the average intensity in the lower right quadrant demonstrates an increase over time as the lower protrusion enters the region. However, the correction algorithm removes the slow trend while retaining the faster fluctuations from mobile mEGFP molecules. The image size is 23.5 μm^2.

bution caused by the bleaching (Fig. 8A). After detrending, however, the recovered brightness is 29,900 cpsm, which falls in the range of values we have measured for such cells (Fig. 8B). Figure 8C displays the average intensity of each frame over the time course of acquisition before and after correction. The bleaching effect is almost entirely eliminated after application of the detrending algorithm.

Although bleaching artifacts could be avoided with careful experimental design, artifacts due to cell protrusion, retraction, or outright cell locomotion are more difficult to avoid. The detrending algorithm we have developed is able to correct for such artifacts, provided the period of the intensity changes due to movement is longer than 10 frames. For example, in Figure 9, a CHO K1 cell expressing mEGFP extended protrusions in two areas during acquisition. The effect on the recovered brightness in those two regions is apparent in the B map (Fig. 9A). After detrending the image stack pixel-by-pixel, the protrusion artifacts are removed. After correction, the B map (Fig. 9B) reports a uniform brightness similar to what we observed in Figures 7B and 8B. A plot of the average intensity in the lower right quadrant of the image stack confirms that the algorithm was successful in removing the increased intensity fluctuations caused by the protrusion while retaining the intensity fluctuations due to the mobile mEGFP molecules (Fig. 9C).

DISCUSSION

We have demonstrated that N&B analysis can be performed on analog systems to recover number count and brightness information with accuracy sufficient to

be useful for both solution and cellular measurements. Most commercially available laser scanning confocal microscopes use analog detection devices (i.e., PMTs), and this analysis should be applicable to data acquired from any such system, thus making available the N&B technique to most researchers in the life sciences. When available, however, N&B determinations are most accurate on photon counting systems.

Characterization of the Analog Detector

The analog detector can be described by three parameters which must be accurately measured for the N&B analysis. The stability of these parameters can be a problem. In our microscope systems, the offset varied by several digital units over 1–2 h. We found that by measuring the dark current after each measurement, we were able to account for most of this variation. Another issue was the nonuniformity of intensity across the field of view. Among different parts of the image, the intensity varied by about 15%, as determined using a slide with a solution of EGFP. Since the brightness measurement depends on the local illumination intensity, the nonuniformity of the field gives a further spread in the brightness histogram. This effect could be corrected by measurement of the changes of intensity across the field of view. However, we found that this correction depends on the scanning speed and other instrument factors.

We studied the effect of the distribution of DL in different detectors. Although the histogram of DL for dark counts varies significantly among detectors, we found that this variation in the distribution does not affect the N&B analysis. The S/N is the only quantity that seems to be affected by this distribution.

A limitation of the analog detector seems to be the small dynamic range. In our system which has a 12-bit A/D converter, the effective dynamic range was less than 20. We estimate that the N&B analysis will be difficult to perform in systems with 8-bit A/D converters. The dynamic range is important in determining the maximum range of brightness that can be measured.

Averaging Neighbor Pixels

The statistics in only one pixel sometimes are insufficient to determine the brightness with enough precision to distinguish a monomer from a dimer. However, the size of the pixel is smaller than the instrument PSF. Averaging several neighboring pixels increases the statistics. We cannot simply average the intensity in the pixels because that will destroy the fluctuations. We separately calculate the B/S image and the intensity image and then we apply a median filter to these two images as described elsewhere (Digman et al., in press). The two filtered images are then used to construct the 2D histogram. The result is now a much sharper histogram in which even small changes in brightness are recognizable. The cursor then selects regions of the 2D histogram and the corresponding pixels in the image are highlighted. It is a property of the median filter not to smear the image. On the contrary, the image appears sharper and the regions with different degrees of aggregation are better visualized.

Pixel Dwell Time

The pixel dwell time must be selected such that molecular fluctuations are accurately recorded. A general guideline is for the dwell time to be about 10 times smaller than the characteristic decay time of the fluctuating molecule. Long dwell times will average out the fluctuations, such that the measured variance will decrease and the recovered brightness will be underestimated. The characteristic decay time can be estimated using the following equation:

$$\tau_D = \frac{\omega^2}{4D} \tag{12}$$

where ω represents the laser beam waist and D is the diffusion coefficient of the molecule. For example, if we have a beam waist of 0.3 μm, then the τ_D of fluorescein and mEGFP in solution will be 75 μs and 250 μs, respectively. A pixel dwell time of 8 μs will satisfy the factor of 10 requirement mentioned earlier in all cases.

Multiple Species of Different Brightness

In many biological samples, multiple species with different brightness values will be present simultaneously and will contribute to the recorded fluctuations. It is possible to obtain the brightness of each such species only if they are spatially separated, such that fluctuations from multiple species do not arise from the same pixel location. Otherwise, the measured brightness will be a weighted sum of the square of the brightness of each species that is present in the pixel. The following equation (Chen et al., 2000, 2003) provides the apparent brightness resulting from multiple species:

$$\varepsilon_{\text{app}} = \frac{\sum_i \varepsilon_i^2 n_i}{\sum_i \varepsilon_i n_i} \tag{13}$$

where n_i represents the average number of molecules of each species in the pixel.

Visualizing the Immobile Fraction

Data representation using a 2D histogram appears to be the most appropriate to visualize locations in the cell where protein aggregation occurs and to quantify the degree of aggregation. In this histogram we plot in the y axis the value of the pixel ratio B/S and in the x axis the value of the pixel intensity. For all pixels with only an immobile fraction, this ratio is 1. By selecting these pixels in the 2D histogram with the cursor, we can highlight the regions made mainly of immobile fraction. If we calibrate the y scale using a solution of EGFP (or any other protein being imaged) we can determine whether there are pixels that have values of brightness equal to the monomer or of larger values in the 2D histogram. Since the presence of immobile fraction can only decrease the value of the brightness determined from this plot, we can establish a lower limit for the degree of aggregation in each pixel. At the borders of regions between mobile and immobile fraction there is a trail of pixels (in the 2D histogram) from one value of B/S characteristic of the mobile fraction to

$B/S = 1$. If we select that part of the histogram, we map the borders of the immobile regions.

Bleaching Correction

We have presented a correction routine which removes the effect of the increased variance on the brightness due to slow changes in intensity (mainly photobleaching, but membrane motion or stage drift can also contribute). If not corrected, bleaching will make some pixels appear brighter than they would be otherwise. Bleaching occurs when immobile components are present, since mobile molecules in a given observation volume are quickly replaced with other mobile molecules. If only the immobile fraction is present, the N&B analysis will normally recover a B/S value of 1. However, the extra variance due to bleaching will cause these pixels to have $B/S > 1$, exactly the artifact which we would like to avoid. The correction routine will restore a value of $B/S = 1$ for these pixels. When both mobile and immobile components are present within the same pixel, the recovery of the true particle number and brightness of the mobile component requires the knowledge in the pixel of the intensity of the immobile part [see Eqs. (9) and (10)]. If bleaching is present, an extra variance term will appear which will result in the B/S value of the immobile fraction becoming larger than 1. The correction routine will then reassign a B/S value of 1 to the immobile part and leave the brightness of the mobile part unchanged.

Comparison With Raster-Scan Image Correlation Spectroscopy

The N&B analysis holds several advantages over correlation-based methods for brightness (and hence aggregation state) determination. Unlike raster-scan image correlation spectroscopy (RICS) (Digman et al., 2005), N&B does not rely on spatial averaging (averaging neighbor pixels to obtain the $G(0)$ value)). In order to obtain an accurate $G(0)$ value, the RICS approach requires placement of a $2^n \times 2^n$ size box completely inside the area of interest (n is 5 or larger). The N&B analysis, however, has no such requirement because fluctuations in each pixel over time are analyzed for comparatively shorter periods of time. The analysis is computationally fast and does not require specialized correlator cards or other hardware. Additionally, the same data set can be processed using either type of analysis to obtain complementary information (brightness, number of particles, and diffusion coefficients) about the fluorophores in the image. For example, RICS can recover accurate diffusion coefficients even in the presence of large immobile structures, while N&B analysis can recover accurate brightness values at every pixel in the image. There is a fundamental difference between the way the number of particles are determined by the $G(0)$ analysis of the RICS method as compared to the moment analysis. In the RICS method we use the "extrapolated" $G(0)$, which is unaffected by the detector shot noise, and the intensity fluctuations arise from moving the laser from pixel-to-pixel. In the N&B analysis, we need to characterize the detector shot noise and subtract its effect from the measured variance at each pixel. In solution, the two methods give the same values. Also the N&B analysis in solution gives the same results as the $G(0)$ analysis using fluctuation correlation spectroscopy and the n and ε analysis using the photon counting histogram method. The N&B analysis cannot distinguish the presence of multiple species from that of a molecule with the same average properties. This separation, however, can be achieved by using the photon counting histogram method, which utilizes the full photon count distribution instead of only the first two moments of the distribution.

Future Developments

Further refinements to the N&B are currently underway to allow more researchers access to this powerful technique. In this paper we have only presented data using one channel. The N&B analysis technique can be used on several channels simultaneously, provided that each detector is independently characterized using the dark current method. The use of N&B with fast-camera based imaging systems is currently being investigated and has the potential to allow quantification of dynamics on the timescale of the camera frame rate. The ability to couple camera based imaging with optical techniques such as TIRF or DIC will further expand the list of research areas which can benefit from the N&B analysis. For example, the mechanism of adhesion formation during cell migration is currently an area of intense investigation, which is often performed on camera-based TIRF systems. N&B applied to such systems will likely reveal the aggregation state of various adhesion proteins at different stages of adhesion maturation. Similar possibilities exist in other areas of cell biology and cellular engineering.

ACKNOWLEDGMENTS

Thanks to Drs. Claire Brown and Jay Unruh for helpful discussions regarding the data acquisition and sample preparation. Additional thanks to Drs. Miguel Vicente-Manzanares, Anjana Nayal, and Donna Webb for helpful discussions regarding the molecular biology and cell culture.

REFERENCES

Chen Y, Muller JD, So PT, Gratton E. 1999. The photon counting histogram in fluorescence fluctuation spectroscopy. Biophys J 77:553–567.

Chen Y, Muller JD, Tetin SY, Tyner JD, Gratton E. 2000. Probing ligand protein binding equilibria with fluorescence fluctuation spectroscopy. Biophys J 79:1074–1084.

Chen Y, Muller JD, Ruan Q, Gratton E. 2002. Molecular brightness characterization of EGFP in vivo by fluorescence fluctuation spectroscopy. Biophys J 82(1, Part 1):133–144.

Chen Y, Wei LN, Muller JD. 2003. Probing protein oligomerization in living cells with fluorescence fluctuation spectroscopy. Proc Natl Acad Sci USA 100:15492–15497.

Digman MA, Brown CM, Sengupta P, Wiseman PW, Horwitz AR, Gratton E. 2005. Measuring fast dynamics in solutions and cells with a laser scanning microscope. Biophys J 89:1317–1327.

Digman MA, Dalal RB, Horwitz AF, Gratton E. Mapping the number of molecules and brightness in the laser scanning microscope. Biophys J, in press.

Kim M, Carman CV, Yang W, Salas A, Springer TA. 2004. The primacy of affinity over clustering in regulation of adhesiveness of the integrin $\alpha L\beta 2$. J Cell Biol 167:1241–1253.

Laukaitis CM, Webb DJ, Donais K, Horwitz AF. 2001. Differential dynamics of α 5 integrin, paxillin, and α-actinin during formation and disassembly of adhesions in migrating cells. J Cell Biol 153:1427–1440.

Miyamoto S, Akiyama SK, Yamada KM. 1995. Synergistic roles for receptor occupancy and aggregation in integrin transmembrane function. Science 267:883–885.

Moriki T, Maruyama H, Maruyama IN. 2001. Activation of preformed EGF receptor dimers by ligand-induced rotation of the transmembrane domain. J Mol Biol 311:1011–1026.

Schlessinger J. 2000. Cell signaling by receptor tyrosine kinases. Cell 103:211–225.

Shi Q, Boettiger D. 2003. A novel mode for integrin-mediated signaling: Tethering is required for phosphorylation of FAK Y397. Mol Biol Cell 14:4306–4315.

Wiseman PW, Brown CM, Webb DJ, Hebert B, Johnson NL, Squier JA, Ellisman MH, Horwitz AF. 2004. Spatial mapping of integrin interactions and dynamics during cell migration by image correlation microscopy. J Cell Sci 117(Part 23):5521–5534.

Zacharias DA, Violin JD, Newton AC, Tsien RY. 2002. Partitioning of lipid-modified monomeric GFPs into membrane microdomains of live cells. Science 296:913–916.